

**Spin dynamics of  $\text{Fe}_7M$  ( $M=\text{Zn},\text{Mn}$ ) heterometallic rings probed by neutron spectroscopy**T. Guidi,<sup>1,2,\*</sup> J. R. D. Copley,<sup>1</sup> Y. Qiu,<sup>1,3</sup> S. Carretta,<sup>4</sup> P. Santini,<sup>4</sup> G. Amoretti,<sup>4</sup> G. Timco,<sup>5</sup> R. E. P. Winpenny,<sup>5</sup> C. L. Dennis,<sup>1</sup> and R. Caciuffo<sup>6</sup><sup>1</sup>*National Institute of Standards and Technology, Gaithersburg, Maryland 20899, USA*<sup>2</sup>*Dipartimento di Fisica ed Ingegneria dei Materiali e del Territorio, Università Politecnica delle Marche, Via Brecce Bianche, I-60131 Ancona, Italy*<sup>3</sup>*Department of Materials Science and Engineering, University of Maryland, College Park, Maryland 20742, USA*<sup>4</sup>*Dipartimento di Fisica, Università di Parma, I-43100 Parma, Italy*<sup>5</sup>*School of Chemistry, The University of Manchester, Oxford Road, Manchester M13 9PL, United Kingdom*<sup>6</sup>*European Commission, Joint Research Centre, Institute for Transuranium Elements, Postfach 2340, D-76125 Karlsruhe, Germany*

(Received 27 September 2006; revised manuscript received 15 November 2006; published 9 January 2007)

The spin dynamics of two representative members of a family of Fe-based heterometallic antiferromagnetic wheels have been investigated by inelastic neutron scattering (INS). The INS spectra measured at various temperatures have been reproduced using microscopic spin Hamiltonians that contain all the main interactions present in the molecules (isotropic exchange, intramolecular dipolar interaction and local crystal fields). The positions of the observed excitations provide evidence of weak second-nearest neighbor antiferromagnetic exchange interactions. Information about the symmetry of the molecular eigenstates has been obtained by studying the momentum-transfer dependence of the intensities of the observed transitions. The results have also been exploited to investigate the time autocorrelation of the Néel vector in these antiferromagnetic wheels. We have shown that  $S$  mixing has a remarkable effect on the Néel vector dynamics and that the tunneling picture is only very approximately valid for these heterometallic rings.

DOI: [10.1103/PhysRevB.75.014408](https://doi.org/10.1103/PhysRevB.75.014408)

PACS number(s): 75.45.+j, 75.10.Jm, 75.50.Tt, 75.40.Gb

**I. INTRODUCTION**

One of the best examples of noninteracting quantum objects embedded in a solid state environment is provided by magnetic molecules. In particular, much interest has been attracted by molecules containing transition-metal ions whose spins are so strongly exchange coupled that at low temperature each molecule behaves like a single-domain particle with fixed total spin  $S$ . Indeed, these systems are appealing both for fundamental physics and for envisaged applications. From a fundamental point of view, these zero-dimensional magnetic units can be considered model systems to investigate quantum phenomena like quantum tunneling of the magnetization. Moreover, being mesoscopic objects, these molecules also offer the possibility to study the transition between the quantum and classical regimes. As far as potential applications are concerned, properly engineered magnetic molecules could be used to realize high-density information storage devices and to implement quantum computation algorithms.<sup>1-4</sup>

Very recently, a particular family of magnetic molecules has attracted considerable attention: Antiferromagnetic (AF) heterometallic  $\text{Cr}_7M$  rings.<sup>1,4-13</sup> The ancestor of this family is a homometallic  $\text{Cr}_8$  ring with AF exchange interactions between the  $\text{Cr}^{3+}$  ( $s=3/2$ ) ions so that the ground state has total spin  $S=0$ .<sup>14,15</sup> Another strategy was used to synthesize heterometallic octanuclear  $\text{Cr}_7M$  wheels in which, alongside seven octahedrally coordinated  $\text{Cr}^{3+}$  ions, there is a divalent transition metal  $M^{2+}$  ion.<sup>16</sup> The breaking of the  $\text{Cr}_8$  ring spin topology, which can be regarded as the replacement of one trivalent  $\text{Cr}^{3+}$  ( $s=3/2$ ) ion with a divalent ion ( $M^{2+}$ ), leads to the opening of new  $S$  mixing channels and to the appearance of quantum oscillations of the total spin length at anticross-

ings between different  $S$  multiplets.<sup>17</sup> These zero-temperature oscillations are particularly interesting since their frequencies can be tuned from zero to tens of GHz simply by changing the direction of the applied field. Therefore, this phenomenon offers the possibility to study the transition from a coherent to an incoherent regime. On the other hand, the topology breaking allows magnetic properties to be tailored to the envisaged application. For instance, we have shown<sup>11</sup> that the  $\text{Cr}_7\text{Cd}$  cluster (having an almost isotropic  $S=3/2$  ground state) could be exploited as a low-temperature magnetocaloric refrigerant. Most importantly, we have shown that  $\text{Cr}_7\text{Ni}$  is very promising for qubit implementation. In fact, this heterometallic wheel is characterized by an energetically isolated  $S=1/2$  ground multiplet that can be safely used to encode a qubit.<sup>10</sup> Moreover, the use of the excited states allows the implementation of time-dependent two-qubit couplings even in the presence of permanent microscopic exchange interactions. It is important to stress that a profound understanding of the molecular spin Hamiltonian is crucial for all of these issues.

An important step forward is to study the family of heterometallic ferric wheels.<sup>16</sup> The synthetic procedure used for heterometallic  $\text{Cr}_7M$  compounds<sup>5</sup> has been extended to another family of heterometallic  $\text{Fe}_7M$  rings.<sup>16</sup> As far as envisaged applications are concerned, the  $\text{Fe}_7\text{Zn}$  AF ring, being characterized by a large half-integer ground multiplet ( $S=5/2$ ), should display a stronger magnetocaloric effect than  $\text{Cr}_7\text{Cd}$ . In addition, this family of compounds might also be promising for quantum information processing. From a fundamental point of view, the rather high value of the spin of  $\text{Fe}^{3+}$ ,  $s=5/2$ , significantly affects the molecular spin dynamics with respect to the  $\text{Cr}_7M$  family of compounds (e.g., the correlation length changes). Hence the comparison between

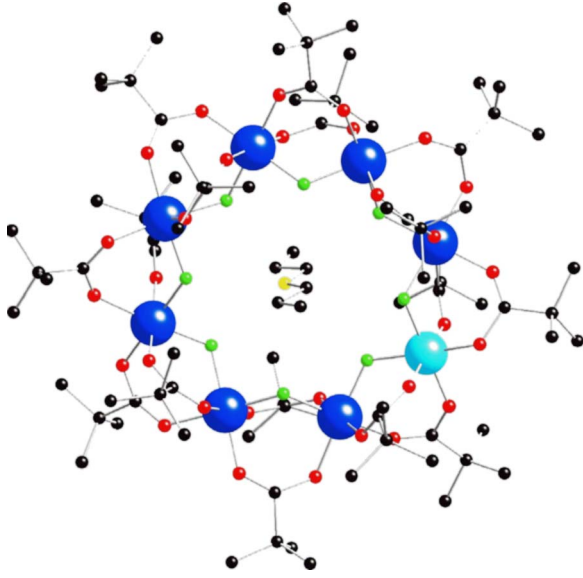


FIG. 1. (Color online) Molecular structure of the AF wheel  $[(C_3H_7)_2NH_2][Fe_7MnF_8\{O_2CC(CD_3)_3\}_{16}]$ . Color scheme: Fe, blue (large dark circles); Mn, cyan (large light circle); F, green (small light circles); O, red (small dark circles); C, black; N, in the ring cavity, yellow (light gray). Hydrogen atoms are omitted for clarity. The Mn position is disordered on the Fe sites.

results obtained for the two families of AF rings can also shed more light on the physics of finite AF spin chains. Furthermore, heterometallic ferric wheels have also been suggested as good candidates for the observation of the so-called tunneling of the Néel vector  $\mathbf{n}$ <sup>7</sup>.

The starting point to address all these issues is the determination of the molecular spin Hamiltonian  $H$ . To achieve this aim, inelastic neutron scattering (INS) is the technique of choice, since it provides direct access to the energies and wave functions of  $H$ . Here we report on INS measurements carried out on two heterometallic ferric wheels with chemical formula  $[(C_3H_7)_2NH_2][Fe_7MnF_8\{O_2CC(CD_3)_3\}_{16}]$ , where  $M = Zn, Mn$  (Fig. 1).

The analysis of the experimental data has enabled an accurate determination of the principal microscopic interactions present in the molecules. In addition, we have studied the Néel vector dynamics by calculating the time correlation function of  $\mathbf{n}$  using the eigenstates and eigenfunctions determined from neutron spectroscopy.

## II. MODEL SPIN HAMILTONIAN

Magnetic properties of AF heterometallic ferric wheels can be modeled using spin Hamiltonians of the form

$$\begin{aligned}
 H = & \left[ \sum_{i=1}^6 J_{Fe-Fe} \mathbf{s}_i \cdot \mathbf{s}_{i+1} + J_{Fe-M} (\mathbf{s}_7 \cdot \mathbf{s}_8 + \mathbf{s}_8 \cdot \mathbf{s}_1) \right. \\
 & \left. + \sum_{i=1}^8 J_{i(i+2)} \mathbf{s}_i \cdot \mathbf{s}_{i+2} \right] + \sum_{i=1}^8 \mathbf{s}_i \cdot \mathbf{D}_i \cdot \mathbf{s}_i + \sum_{i<j=1}^8 \mathbf{s}_i \cdot \mathbf{D}_{ij} \cdot \mathbf{s}_j \\
 & + \mu_B \sum_{i=1}^8 g_i \mathbf{B} \cdot \mathbf{s}_i,
 \end{aligned} \quad (1)$$

where  $\mathbf{s}_i$  are spin operators of the  $i$ th magnetic ion in the molecule. Ring sites  $i=1-7$  contain  $Fe^{3+}$  ions ( $s=5/2$ ), while the  $i=8$  ring site is occupied by the  $M$  ion. The term in brackets is the nearest-neighbor and next nearest-neighbor isotropic Heisenberg exchange interaction (with  $\mathbf{s}_{9(10)} \equiv \mathbf{s}_{1(2)}$ ,  $J_{7-9} \equiv J_{7-1}$ , and  $J_{8-10} \equiv J_{8-2}$ ).  $J_{Fe-Fe}$  and  $J_{Fe-M}$  are the Fe-Fe and Fe- $M$  exchange integrals, respectively. The second term describes the interaction with local crystal-fields (CFs) and the third term is the dipole-dipole intracluster interaction, which is evaluated within the point-dipole approximation. The final term is the Zeeman coupling to an external magnetic field  $\mathbf{B}$ . As far as the CF interaction is concerned, we assume nearly uniaxial magnetic anisotropy and we consider the axial and rhombic terms only:<sup>12</sup>

$$\sum_{i=1}^8 \mathbf{s}_i \cdot \mathbf{D}_i \cdot \mathbf{s}_i = \sum_{i=1}^8 d_i \left[ s_{z,i}^2 - \frac{1}{3} s_i(s_i+1) \right] + \sum_{i=1}^8 e_i [s_{x,i}^2 - s_{y,i}^2], \quad (2)$$

where the  $\hat{z}$  axis is perpendicular to the ring plane. The dimension of the spin Hilbert space of the rings studied in the present work is rather large (e.g., 1679616 for  $Fe_7Mn$ ). The most important  $S$  mixing effects have been included in the calculations by the two-step procedure described in Refs. 18 and 19. Finally, the INS cross section for a polycrystalline sample is<sup>12</sup>

$$\frac{\partial^2 \sigma}{\partial \Omega \partial (\hbar \omega)} = \frac{A}{N_m k_0} e^{-2W} \sum_{n,n'} \frac{e^{-\beta E_n}}{Z} I_{nn'}(\mathbf{Q}) \delta(\hbar \omega - E_{n'} + E_n), \quad (3)$$

where  $A=0.29$  b,  $\beta=1/(k_B T)$ , and the function  $I_{nn'}(\mathbf{Q})$  is defined as

$$\begin{aligned}
 I_{nn'}(\mathbf{Q}) = & \sum_{i,j} F_i^*(\mathbf{Q}) F_j(\mathbf{Q}) \left\{ \frac{2}{3} [j_0(QR_{ij}) + C_0^2 j_2(QR_{ij})] \tilde{s}_{z_i} \tilde{s}_{z_j} \right. \\
 & + \frac{2}{3} \left[ j_0(QR_{ij}) - \frac{1}{2} C_0^2 j_2(QR_{ij}) \right] (\tilde{s}_{x_i} \tilde{s}_{x_j} + \tilde{s}_{y_i} \tilde{s}_{y_j}) \\
 & + \frac{1}{2} j_2(QR_{ij}) [C_2^2 (\tilde{s}_{x_i} \tilde{s}_{x_j} - \tilde{s}_{y_i} \tilde{s}_{y_j}) + C_{-2}^2 (\tilde{s}_{x_i} \tilde{s}_{y_j} + \tilde{s}_{y_i} \tilde{s}_{x_j})] \\
 & \left. + j_2(QR_{ij}) [C_1^2 (\tilde{s}_{z_i} \tilde{s}_{x_j} + \tilde{s}_{x_i} \tilde{s}_{z_j}) + C_{-1}^2 (\tilde{s}_{z_i} \tilde{s}_{y_j} + \tilde{s}_{y_i} \tilde{s}_{z_j})] \right\}, \quad (4)
 \end{aligned}$$

$N_m$  is the number of magnetic ions,  $Z$  is the partition function,  $\mathbf{k}_f$  and  $\mathbf{k}_0$  are the wave vectors of the scattered and incident neutrons,  $\exp(-2W)$  is the Debye-Waller factor,  $\mathbf{Q} = \mathbf{k}_0 - \mathbf{k}_f$  is the scattering vector,  $E_n$  is the energy of the generic spin state  $|n\rangle$ ,  $F(\mathbf{Q})$  is the single-ion magnetic form factor, and  $\mathbf{R}_{ij}$  gives the relative position of ions  $i$  and  $j$ . In addition

$$C_0^2 = \frac{1}{2} \left[ 3 \left( \frac{R_{ijz}}{R_{ij}} \right)^2 - 1 \right],$$

$$\begin{aligned}
C_2^2 &= \frac{R_{ijx}^2 - R_{ijy}^2}{R_{ij}^2}, \\
C_{-2}^2 &= 2 \frac{R_{ijx}R_{ijy}}{R_{ij}^2}, \\
C_1^2 &= \frac{R_{ijx}R_{ijz}}{R_{ij}^2}, \\
C_{-1}^2 &= \frac{R_{ijy}R_{ijz}}{R_{ij}^2},
\end{aligned} \quad (5)$$

and

$$\tilde{s}_{\alpha_i} \tilde{s}_{\gamma_j} = \langle n | s_{\alpha_i} | n' \rangle \langle n' | s_{\gamma_j} | n \rangle \quad (\alpha, \gamma = x, y, z). \quad (6)$$

### III. EXPERIMENTAL DETAILS

A wide variety of heterometallic wheel complexes have recently been synthesized with the general formula  $(R_2\text{NH}_2)[M_7M'\text{F}_8(\text{O}_2\text{CCR}')_{16}]$  where  $M=\text{V(III)}$ ,  $\text{Cr(III)}$ , or  $\text{Fe(III)}$ ,  $M'=\text{Ni(II)}$ ,  $\text{Co(II)}$ ,  $\text{Mn(II)}$ ,  $\text{Fe(II)}$ ,  $\text{Zn(II)}$ ,  $\text{Cd(II)}$ , or  $\text{Mg(II)}$ ,  $R$  is a linear alkyl chain, e.g.,  $n$ -propyl, and  $\text{O}_2\text{CCR}'$  is one of twenty possible carboxylates.<sup>16</sup>

Partially deuterated microcrystalline samples of  $[(\text{C}_3\text{H}_7)_2\text{NH}_2][\text{Fe}_7\text{MF}_8\{\text{O}_2\text{CC}(\text{CD}_3)_3\}_{16}]$ , where  $M=\text{Zn}$  (in short  $\text{Fe}_7\text{Zn-}d$ ) and  $M=\text{Mn}$  (in short  $\text{Fe}_7\text{Mn-}d$ ) have been prepared according to a slightly modified literature procedure<sup>16</sup> by dissolving iron(III) fluoride trihydrate in a mixture of trimethyl- $d_9$ -acetic acid and dipropylamine before adding an excess of the second metal salt, basic zinc carbonate, or manganese chloride tetrahydrate.  $\text{Fe}_7\text{Zn-}d$  and  $\text{Fe}_7\text{Mn-}d$  were crystallized from pentane and then dried *in vacuo*. Elemental analysis and electrospray mass spectrometry (ES MS) confirmed the chemical compositions of both compounds. The homometallic wheel  $\text{Fe}_8\text{F}_8\{\text{O}_2\text{CC}(\text{CD}_3)_3\}_{16}$  ( $\text{Fe}_8-d$  in short) was detected by ES MS as a 4% impurity in the  $\text{Fe}_7\text{Zn-}d$ . Due to the practically identical solubilities of  $\text{Fe}_7\text{Zn}$  and  $\text{Fe}_8$  it was not possible to remove this impurity by recrystallization. The preparation of trimethyl- $d_9$ -acetic acid starting from acetone- $d_6$  was adapted from standard methods.<sup>20</sup>

Susceptibility measurements were performed using a superconducting quantum-interference-device (SQUID) magnetometer. Samples were placed in a gelatin capsule and magnetization measurements were performed in a fixed field, varying the temperature from 2 to 310 K.

Inelastic neutron scattering measurements were performed using the disk chopper spectrometer (DCS) at the NIST Center for Neutron Research (NCNR), Gaithersburg (USA).<sup>21</sup> The polycrystalline samples were packed under helium into aluminum annular sample cans, 20 mm diameter, 0.7 mm annular thickness, and 100 mm high. The samples were mounted in a standard ILL ‘‘Orange’’ cryostat. The DCS was operated in its ‘‘low resolution’’ mode,<sup>21</sup> using several incident wavelengths, from 3 to 7 Å, and data were recorded at various temperatures between 1.5 and 30 K. The back-

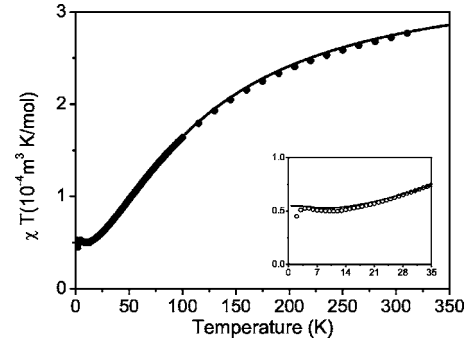


FIG. 2.  $dc\text{-}\chi T$  experimental data for  $\text{Fe}_7\text{Zn}$  measured using an applied field of  $10^7/4\pi$  A/m ( $10^4$  Oe). Note that  $1 \text{ m}^3/\text{mol} = 10^6/4\pi$  emu/mol Oe. The continuous line is calculated using  $J_{i(i+1)} = 1.49$  meV. The inset shows a blowup of the low temperature region. A  $0.038 \times 10^{-6} \text{ m}^3/\text{mol}$  ( $0.003$  emu/mol Oe) diamagnetic contribution to the susceptibility has been added.

ground was subtracted, and detector efficiency corrections were performed using a standard vanadium sample. The spectra were integrated over all of the detectors, covering scattering angles from  $-30^\circ$  to  $-5^\circ$  and from  $5^\circ$  to  $140^\circ$ . The DAVE software package<sup>22</sup> was used to reduce the time-of-flight data.

### IV. EXPERIMENTAL RESULTS

#### A. $\text{Fe}_7\text{Zn}$

The starting point of the work has been  $\text{Fe}_7\text{Zn}$ , which is the simplest compound of the series since  $\text{Zn}^{2+}$  is diamagnetic. The odd number of antiferromagnetically coupled  $\text{Fe}^{3+}$  ions leads to a magnetic  $S=5/2$  ground state. A first estimate of  $J_{\text{Fe-Fe}}$  has been obtained from susceptibility data. The results of a SQUID measurement on 80 mg of protonated  $\text{Fe}_7\text{Zn}$  are shown in Fig. 2. By fitting the experimental data we estimate a value of 1.49 meV for the nearest-neighbor exchange parameter  $J_{\text{Fe-Fe}}$ . The calculated curve is shown in Fig. 2. The upturn at  $\approx 10$  K is due to the magnetic  $S=5/2$  ground multiplet. The low-temperature fall of  $\chi T$  is due to the zero field splitting (ZFS) of the ground manifold.

INS experiments have been performed on a 3.8 g powder sample of  $\text{Fe}_7\text{Zn-}d$ . High resolution experimental data were collected with an incident wavelength of 7 Å [ $42 \mu\text{eV}$  full width at half maximum (FWHM) energy resolution at the elastic peak]. Figure 3 (upper panel) shows spectra collected at two temperatures, 1.5 and 5 K. The two pronounced peaks correspond to the two allowed transitions within the anisotropy-split  $S=5/2$  ground multiplet, i.e., transitions from the  $|S=5/2, M=\pm 5/2\rangle$  ground doublet to the  $|S=5/2, M=\pm 3/2\rangle$  first excited states (lying at about 0.21 meV) and from the latter states to the  $|S=5/2, M=\pm 1/2\rangle$  states (lying at 0.33 meV). The easy-axis nature of the ZFS (i.e., the fact that  $|S=5/2, M=\pm 5/2\rangle$  is the ground doublet) is demonstrated by the temperature dependence of the two peaks. A good fit to the data can be obtained with the crystal-field parameter  $d_{\text{Fe}} = -15 \mu\text{eV}$  and  $|e_{\text{Fe}}/d_{\text{Fe}}| = 0.1$  ( $d_{\text{Zn}} = e_{\text{Zn}} = 0$ ). The calculated curves, shown in Fig. 3 as continuous lines, were obtained using the INS cross section

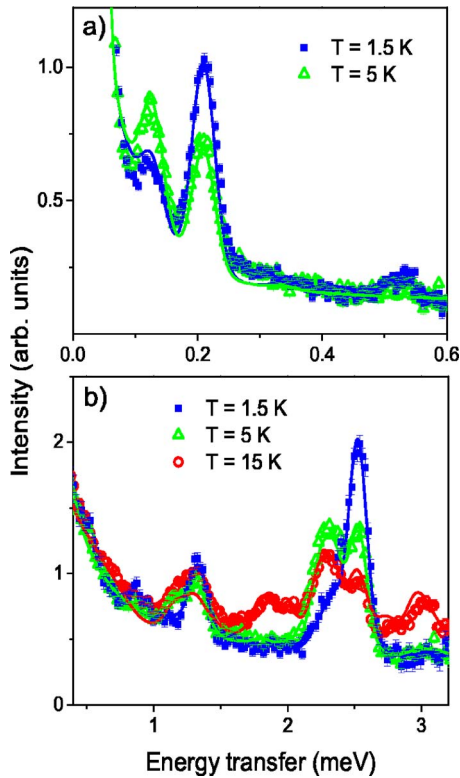


FIG. 3. (Color online) INS intensity measured in  $\text{Fe}_7\text{Zn-d}$  as a function of the energy transfer using wavelengths of 7 Å (upper panel) and 4.5 Å (lower panel). Sample temperatures are 1.5 K (blue squares), 5 K (green open triangles), and 15 K (red open circles). The data were obtained by integrating over the whole detector bank. The solid lines represent calculations described in the text.

formula of Sec. II and associating with each transition a Gaussian line shape with an area proportional to the transition probability. Higher-energy excitations have been observed with an incident wavelength of 4.5 Å (140  $\mu\text{eV}$  FWHM resolution). At the lowest temperature,  $T=1.5$  K, two sharp peaks are visible at 1.3 and 2.5 meV [Fig. 3(b)]. The latter corresponds to transitions from the ground doublet to the lowest  $S=7/2$  excited manifold. It is worth noting that these transitions involve states within the so-called Landé rotational band.<sup>23,24</sup> Instead, the peak at about 1.3 meV corresponds to a transition involving an excited  $S=3/2$  multiplet which does not belong to the lowest rotational band. The  $Q$  dependence of the two different types of excitations is shown in Fig. 4.

As the temperature is raised to 5 K, transitions from the excited levels of the anisotropy split ground state multiplet lead to peaks growing as lower-energy shoulders. They reflect the lifting of the ground state degeneracy by the anisotropy and confirm our interpretation. Finally, at 15 K excited manifolds are populated and transitions between excited multiplets appear. Intermultiplet excitations can be well reproduced with  $J_{i(i+1)}=1.35$  meV and  $J_{i(i+2)}/J_{i(i+1)}=0.016$ . A weak antiferromagnetic second nearest-neighbor exchange interaction is needed to account for the position of the peak at 1.3 meV, which is expected at significantly higher energy if  $J_{i(i+2)}=0$ . Indeed, the structure of the  $S=3/2$  excited mul-

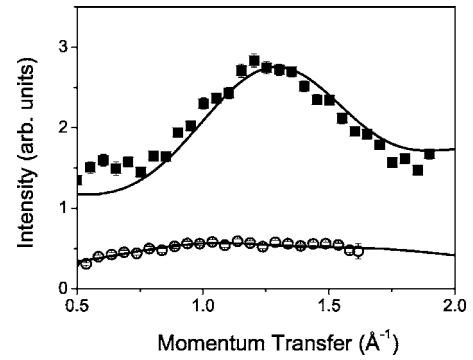


FIG. 4. Intensity vs  $Q$  dependence of the observed peaks at 0.21 meV (squares) and 1.3 meV (open circles) ( $T=1.5$  K) recorded using  $\lambda=6$  Å incident wavelength. The continuous lines represent the theoretical calculations.

tiplet at 1.3 meV makes its energy particularly sensitive to the second nearest-neighbor exchange interaction. The spin eigenstate energy level scheme calculated assuming only isotropic exchange interactions is shown in Fig. 5.

The lowest temperature spectra in Fig. 3 include inelastic features at about 0.53 and 0.9 meV that cannot be described with the model spin Hamiltonian. To understand the origin of these two peaks we performed an INS measurement using 6 Å incident wavelength (64  $\mu\text{eV}$  FWHM resolution). The intensity and temperature dependence of the two excitations provide clear evidence of their magnetic origin. Moreover, their temperature dependence indicates that they originate from the ground state of the system (see Fig. 6). The most likely explanation for the appearance of these two extra peaks is that there is a small percentage of impurity in the  $\text{Fe}_7\text{Zn-d}$  sample, namely the homonuclear analog  $\text{Fe}_8-d$ . The  $\text{Fe}_7\text{Zn}$  compound is indeed the least stable in the series of  $\text{Fe}_7M$  rings, and  $\text{Fe}_8$  impurities were also found through mass spectrometry measurements, as reported above. The  $\text{Fe}_8$  system, due to the full compensation of the antiferromagnetically interacting spins, has an  $S=0$  ground state. Hence the two excitations at 0.53 and 0.9 meV should correspond to the transition to the first anisotropy split  $S=1$  excited state. Numerical calculations based on the assumption of some  $\text{Fe}_8-d$  impurity, with practically the same parameters as the  $\text{Fe}_7\text{Zn-d}$  analog, are consistent with the complete set of ex-

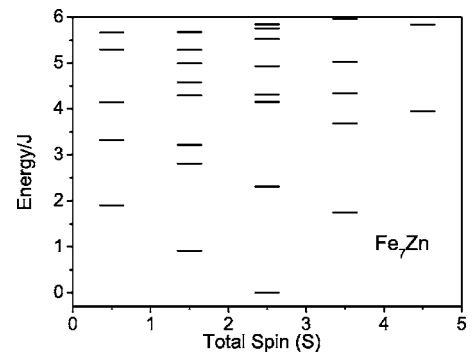


FIG. 5. Calculated energy levels as a function of the total spin  $S$  for  $\text{Fe}_7\text{Zn}$  assuming only isotropic exchange interactions ( $J = J_{i(i+1)} = 1.35$  meV and  $J_{i(i+2)}/J_{i(i+1)} = 0.016$ ).

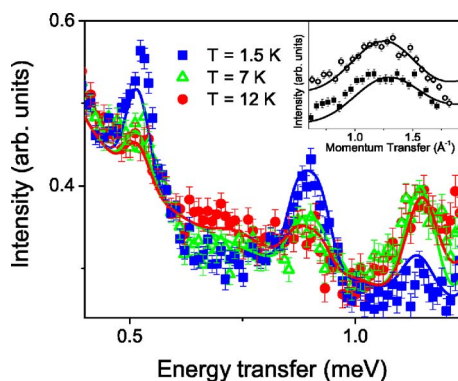


FIG. 6. (Color online) INS energy loss spectra for  $\text{Fe}_7\text{Zn-d}$  recorded using  $\lambda=6$  Å incident wavelength. The sample temperature is 1.5 K (blue squares), 7 K (green open triangles), and 12 K (red circles). The solid lines represent theoretical curves calculated including contributions from both  $\text{Fe}_7\text{Zn-d}$  and  $\text{Fe}_8-d$ , and using the spin Hamiltonian parameters given in the text. The inset shows the intensity vs  $Q$  dependence of the observed peaks at 0.53 meV (open circles) and 0.9 meV (squares) ( $T=1.5$  K) compared with the calculation (continuous lines).

perimental data at different temperatures and incident energies. The most intense excitations originating from the  $\text{Fe}_8-d$  phase are the  $|S=0\rangle \rightarrow |S=1\rangle$  transitions which are well described by the proposed model, as shown by the continuous lines of Fig. 6. From a simultaneous fit of both phases of the sample, we obtained an estimate of the mass fraction of  $\text{Fe}_8-d$ , about 4%, in excellent agreement with the elemental analysis and electro-spray mass-spectrometry results. Further confirmation of the appropriate assignment of the observed excitations is given by the favorable comparison between calculated and measured intensity vs  $Q$  curves (see inset to Fig. 6). This finding could also explain the apparent large diamagnetism which had to be assumed in order to fit the susceptibility data.

### B. $\text{Fe}_7\text{Mn}$

The  $\text{Fe}_7\text{Mn}$  wheel contains 7  $\text{Fe}^{3+}$  ions and one  $\text{Mn}^{2+}$  (high spin  $s=5/2$ ) ion. Being composed of an even number of antiferromagnetically coupled  $s=5/2$  ions, it is characterized by a nonmagnetic  $S=0$  ground state. Susceptibility measurements on  $\text{Fe}_7\text{Mn}$  (Fig. 7) have been performed on a 70 mg partially deuterated powder sample. A good fit to the experimental data is obtained with a single  $J_{i(i+1)}=1.62$  meV exchange parameter.

3.9 g of the partially deuterated  $\text{Fe}_7\text{Mn-d}$  powder sample were used for the INS measurements. With an incident wavelength of 6 Å we observed two sharp resolution-limited inelastic peaks at 1.5 K with energy transfers of about 0.5 and 0.9 meV [Fig. 8(a)]. The intensities of both peaks decrease with increasing temperature according to the Boltzmann factor, suggesting that the excitations can be assigned to transitions from the  $|S=0\rangle$  ground state to the anisotropy-split  $|S=1\rangle$  states. A higher energy peak, at  $\sim 1.3$  meV and corresponding to transitions between excited multiplets, appears at higher temperatures. Assuming site-independent exchange

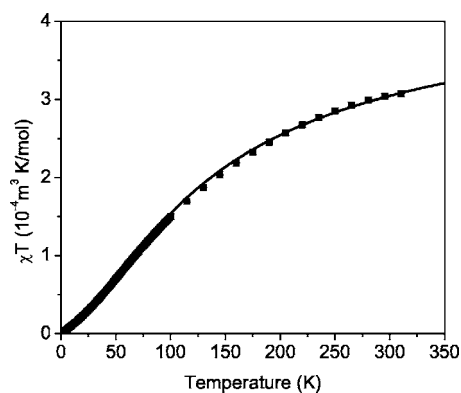


FIG. 7.  $dc\text{-}\chi T$  measurements for  $\text{Fe}_7\text{Mn}$  taken with an applied field of  $10^6/4\pi$  A/m ( $10^3$  Oe). Note that  $1 \text{ m}^3/\text{mol}=10^6/4\pi$  emu/mol Oe. The calculated curve (continuous line) was obtained using  $J_{i(i+1)}=1.62$  meV.

and anisotropy parameters, the experimental data are well reproduced using the same anisotropy parameters as were used in  $\text{Fe}_7\text{Zn}$  (see Fig. 8). As far as exchange interactions are concerned, the ratio  $J_{i(i+2)}/J_{i(i+1)}$  was fixed at 0.016 as in  $\text{Fe}_7\text{Zn}$ , and we have found that  $J_{i(i+1)}=1.42$  meV, slightly higher than in  $\text{Fe}_7\text{Zn}$ . This might indicate that  $J_{\text{Fe-Mn}}$  is somewhat larger than  $J_{\text{Fe-Fe}}$ . Indeed, by fixing  $J_{\text{Fe-Fe}}$  to the value determined in  $\text{Fe}_7\text{Zn}$  we have found  $J_{\text{Fe-Mn}}=1.7$  meV. Figure 8(b) shows spectra collected with  $\lambda=4.5$  Å at three

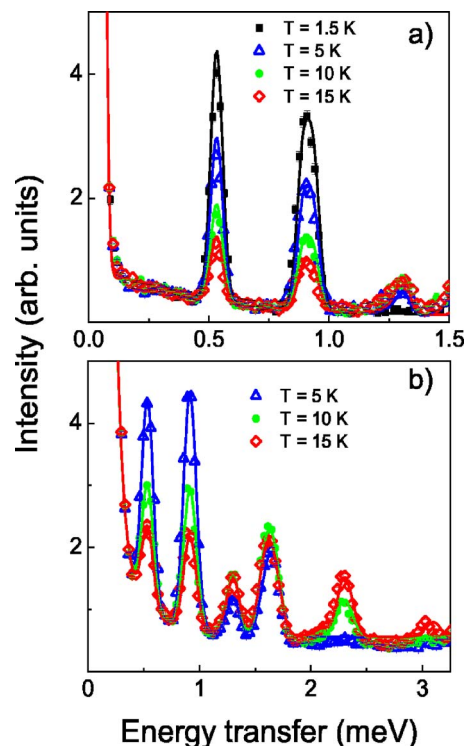


FIG. 8. (Color online) Neutron energy loss spectra for  $\text{Fe}_7\text{Mn}$  measured with (a) 6 Å ; and (b) 4.5 Å incident wavelengths at  $T=1.5$  (black squares), 5 (blue open triangles), 10 (green circles), and 15 K (red open diamonds). Continuous lines are spectra calculated using the spin Hamiltonian, Eq. (1), with the parameters determined in the present work (see main text).

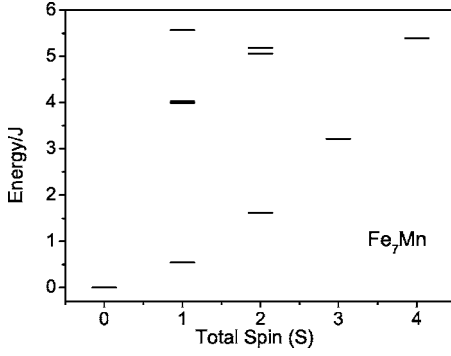


FIG. 9. Calculated energy levels as a function of the total spin  $S$  for the  $\text{Fe}_7\text{Mn}$  compound. Only isotropic exchange interactions are assumed in the calculation, with  $J=J_{i(i+1)}=1.42$  meV and  $J_{i(i+2)}/J_{i(i+1)}=0.016$ .

temperatures, namely 5, 10, and 15 K, where transitions involving excited states are clearly visible. For instance, the two peaks at about 1.3 and 1.6 meV correspond to transitions between the  $S=1$  and  $S=2$  multiplets of the lowest rotational band and the peaks at 2.3 and 3 meV are thermally activated transitions from the  $S=2$  and  $S=3$  excited states, respectively. The calculated energies of the lowest eigenstates as a function of the total spin  $S$  using  $J_{i(i+1)}$  and  $J_{i(i+2)}$  parameters obtained as described above are shown in Fig. 9. The energy and temperature ranges spanned with 6 and 4.5 Å neutrons only allowed us to observe excitations of appreciable intensity within the lowest rotational band, i.e., the so-called “Landé band.”<sup>25</sup> These excitations have a very well defined oscillatory  $Q$  dependence. In Fig. 10, the upper curve (circles) represents the  $Q$  dependence measured for the  $|S=0\rangle \rightarrow |S=1\rangle$  transition at 0.9 meV, showing the typical  $Q$  dependence of an intra-Landé band excitation. Other important information about the symmetry of wavefunctions is provided by higher energy measurements which have been performed using 3 Å neutrons (450  $\mu\text{eV}$  energy resolution). This experimental setup allowed us to observe excitations involving states with different spatial symmetry with respect to the Landé band states. In particular, we have observed a

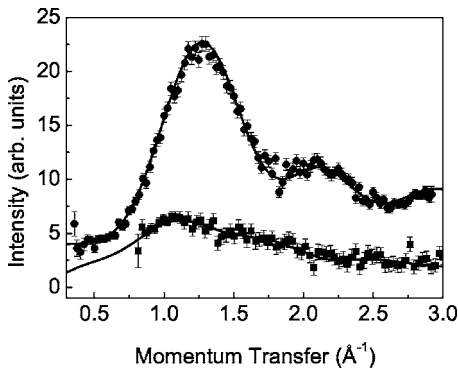


FIG. 10. INS intensity for  $\text{Fe}_7\text{Mn}$  as a function of the momentum transfer  $Q$  for two peaks: A representative intra-Landé band excitation at 0.9 meV (upper curve) and an  $L$ -band to  $E$ -band excitation at 5.4 meV (lower curve). Continuous lines are the corresponding calculated curves.

peak at about 5.4 meV that corresponds to interband transitions from the  $L$ -band ( $|S=0\rangle$ ) to the so-called  $E$ -band ( $|S=1'\rangle$ ).<sup>24,26</sup> The  $Q$ -dependence of the intensity of this excitation exhibits much flatter behavior as compared with the intra-Landé band excitation, as shown in Fig. 10. The good agreement between the calculated curves (continuous lines in Fig. 10) and the experimental data lend additional validity to the model spin Hamiltonian. It should be noted that from INS experimental data of the  $\text{Fe}_7\text{Mn}-d$  compound no evidence of  $\text{Fe}_8-d$  impurity was found, which is also in agreement with its mass spectrum.

## V. NÉEL VECTOR DYNAMICS

One of the most debated aspects of the low-energy spin dynamics of antiferromagnetic rings is the possibility that quantum tunneling of the Néel vector  $\mathbf{n}=\sum_{i=1,N}(-1)^i\mathbf{s}_i/N$ <sup>7,27,28</sup> can be observed. This tunneling is the AF counterpart of the tunneling of the molecular magnetization  $M$  observed in high-spin nanomagnets (e.g.,  $\text{Mn}_{12}$  or  $\text{Fe}_8$ ). In the latter case the tunneling time is macroscopic; indeed so long that the time autocorrelation of  $M$  becomes overdamped due to the interaction with other degrees of freedom. Thus temporal oscillations of  $M$  associated with coherent tunneling do not actually take place. On the other hand, the time scale of the tunneling of  $\mathbf{n}$  in AF rings is expected to be microscopic, much shorter than the decoherence time associated with spin-nuclei or spin-phonon interactions.

We have recently shown that the Néel vector tunneling (NVT) picture applies only very approximately in the candidate homometallic AF rings studied so far.<sup>28</sup> Here we address this issue as it applies to the heterometallic AF rings  $\text{Fe}_7\text{Zn}$  and  $\text{Fe}_7\text{Mn}$ .

In an ideal NVT scenario, the two lowest eigenstates are given by the symmetric and antisymmetric superpositions of the two classical Néel states [i.e.,  $1/\sqrt{2}(|\uparrow, \downarrow, \uparrow, \dots\rangle \pm |\downarrow, \uparrow, \downarrow, \dots\rangle)$ ]. Within a semiclassical framework, this is guaranteed for homometallic AF rings by the condition that the tunnel action  $S_0=Ns\sqrt{-2d/J}$  be much larger than unity<sup>29</sup> ( $d<0$ ). In this case the orientation of the vector  $\mathbf{n}$  tunnels between  $+\hat{z}$  and  $-\hat{z}$ . From a quantum point of view, the dynamics of  $n_z$  can be studied through the zero-temperature autocorrelation:

$$\langle n_\alpha(t)n_\alpha(0) \rangle = \sum_\nu e^{i\Delta_\nu t/\hbar} |\langle \nu | n_\alpha | 0 \rangle|^2, \quad (7)$$

where  $|\nu\rangle$  is the  $\nu$ th energy level and  $\Delta_\nu=E(\nu)-E(0)$ . In principle, many different frequencies contribute to the Néel-vector dynamics. Figure 11 compares the calculated spectral weight  $|\langle 1 | n_z | 0 \rangle|^2$  with the sum of all remaining higher-frequency weights. Whereas in zero field a single frequency dominates the spectrum, this does not hold for  $B \neq 0$ , except when  $B$  is intermediate between two ground-state crossing fields, i.e., corresponding to anticrossings between the first and second excited states. Thus at these particular values of  $B$  (including  $B=0$ ), the autocorrelation of  $n_z$  essentially oscillates with a single frequency. For instance, in  $\text{Fe}_7\text{Mn}$  (Fig. 11) the oscillations are almost monochromatic at  $B=9.8$  T,

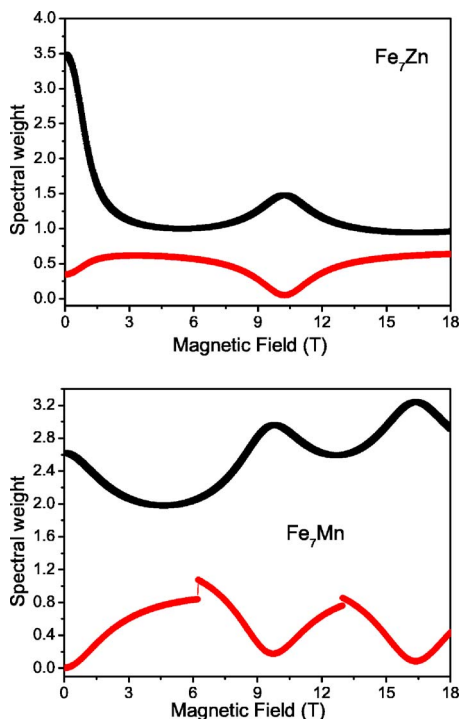


FIG. 11. (Color online) Magnetic-field dependence of  $|\langle 1|n_z|0\rangle|^2$  [black (dark gray) line] compared with  $\sum_{\nu>1}|\langle \nu|n_z|0\rangle|^2$  [red (light gray) line], calculated from the full Hamiltonian Eq. (1) for  $\text{Fe}_7\text{Zn}$  (upper panel) and  $\text{Fe}_7\text{Mn}$  (lower panel) rings. The magnetic field is oriented along  $\hat{x}$ .

between the first two crossing fields  $B_{C_1}=6.2$  T and  $B_{C_2}=13$  T. However, this is not sufficient for the tunneling picture to apply. A more stringent condition is related to the structure of the two lowest eigenstates, i.e., it is necessary to check to what extent they are given by even and odd combinations of the two classical Néel states. In an ideal tunneling scenario the spectral weight  $|\langle 1|n_z|0\rangle|^2$  is equal to  $s^2=6.25$ . This regime would be achieved in the limit  $N^2d \gg J$ . Figure 11 reports the magnetic field dependence of  $|\langle 1|n_z|0\rangle|^2$  calculated with the model derived from the analysis of INS data. Neither in  $\text{Fe}_7\text{Zn}$ , nor in  $\text{Fe}_7\text{Mn}$ , is the tunneling regime truly achieved.<sup>13</sup> Therefore, in both homometallic and heterometallic ferric wheels, the low-energy spin dynamics is only very approximately described by the Néel vector tunneling picture.

Classical states would be recovered only for very large values of  $|d|$ , which implies a large degree of  $S$  mixing. Even for values of  $|d|$  close to the one we have found here,  $S$

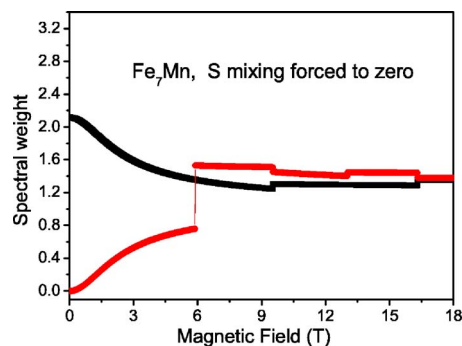


FIG. 12. (Color online) Magnetic-field dependence of  $|\langle 1|n_z|0\rangle|^2$  [black (dark gray) line] compared with  $\sum_{\nu>1}|\langle \nu|n_z|0\rangle|^2$  [red (light gray) line], calculated from the full Hamiltonian Eq. (1) for  $\text{Fe}_7\text{Mn}$ . The calculations were performed with  $S$  mixing forced to zero. The magnetic field is oriented along  $\hat{x}$ .

mixing plays an important role. First of all, at  $B=0$  it increases the weight  $|\langle 1|n_z|0\rangle|^2$  by about 25% in  $\text{Fe}_7\text{Mn}$ . More remarkably, our calculations indicate that for  $B \neq 0$   $S$  mixing produces the single-frequency behavior in between level crossings seen in Fig. 11. In fact, when  $S$  mixing is artificially suppressed, the autocorrelation of  $n_z$  is not characterized by a single-frequency any more (see Fig. 12).

## VI. CONCLUSIONS

The spin dynamics of a family of heterometallic AF ferric wheels have been investigated by neutron spectroscopy. The experimental INS spectra have been reproduced using microscopic spin Hamiltonians which contain all the main interactions present in the molecules. The analysis of INS data has provided evidence of weak second-nearest neighbor antiferromagnetic exchange interactions. The results obtained in the present work show that magnetic properties in ferric wheels can be tailored by chemical substitution of magnetic ions. The Hamiltonian determined herein has been used to investigate the dynamics of the Néel vector  $\mathbf{n}$ . We have found that a tunneling scenario for this observable is only very approximately valid in both homometallic and heterometallic AF ferric wheels.

## ACKNOWLEDGMENTS

This work was partly supported by EC-RTNQUEMOLNA Contract No. nMRTN-CT-2003-504880 and EPSRC(UK). This work utilized facilities supported in part by the National Science Foundation under Grant No. DMR-0454672.

\*Present address: Hahn-Meitner Institut, Glienicker Strasse 100, 14109 Berlin, Germany.

<sup>1</sup>E. J. L. McInnes, S. Piligkos, G. A. Timco, and R. E. P. Winpenny, *Coord. Chem. Rev.* **249**, 2577 (2005).

<sup>2</sup>M. N. Leuenberger and D. Loss, *Phys. Rev. B* **61**, 1286 (2000).

<sup>3</sup>M. N. Leuenberger and D. Loss, *Nature (London)* **410**, 789

(2001).

<sup>4</sup>F. Troiani, M. Affronte, S. Carretta, P. Santini, and G. Amoretti, *Phys. Rev. Lett.* **94**, 190501 (2005).

<sup>5</sup>F. K. Larsen, E. J. L. McInnes, H. E. Mkami, J. Overgaard, S. Piligkos, J. Rajaraman, E. Rentschler, A. A. Smith, G. M. Smith, V. Boote, M. Jennings, G. A. Timco, and R. E. P. Winpenny,

- Angew. Chem., Int. Ed. **42**, 101 (2003).
- <sup>6</sup>F. K. Larsen, J. Overgaard, S. Parsons, E. Rentschler, A. A. Smith, G. A. Timco, and R. E. P. Winpenny, *Angew. Chem., Int. Ed.* **42**, 5978 (2003).
- <sup>7</sup>F. Meier and D. Loss, *Phys. Rev. B* **64**, 224411 (2001).
- <sup>8</sup>F. Meier, J. Levy, and D. Loss, *Phys. Rev. Lett.* **90**, 047901 (2003).
- <sup>9</sup>F. Meier, J. Levy, and D. Loss, *Phys. Rev. B* **68**, 134417 (2003).
- <sup>10</sup>F. Troiani, A. Ghirri, M. Affronte, S. Carretta, P. Santini, G. Amoretti, S. Piligkos, G. Timco, and R. E. P. Winpenny, *Phys. Rev. Lett.* **94**, 207208 (2005).
- <sup>11</sup>M. Affronte, A. Ghirri, S. Carretta, G. Amoretti, S. Piligkos, G. A. Timco, and R. E. P. Winpenny, *Appl. Phys. Lett.* **84**, 3468 (2004).
- <sup>12</sup>R. Caciuffo, T. Guidi, G. Amoretti, S. Carretta, E. Livioti, P. Santini, C. Mondelli, G. Timco, C. A. Muryn, and R. E. P. Winpenny, *Phys. Rev. B* **71**, 174407 (2005).
- <sup>13</sup>S. Carretta, P. Santini, G. Amoretti, T. Guidi, J. R. D. Copley, Y. Qiu, R. Caciuffo, G. Timco, and R. E. P. Winpenny (unpublished).
- <sup>14</sup>N. V. Gerbelev, Y. T. Struchkov, G. A. Timco, A. S. Batsanov, K. M. Indrichan, and G. A. Popovich, *Dokl. Akad. Nauk SSSR* **313**, 1459 (1990).
- <sup>15</sup>J. van Slageren, R. Sessoli, D. Gatteschi, A. A. Smith, M. Hellinwell, R. E. P. Winpenny, A. Cornia, A.-L. Barra, A. G. M. Jansen, E. Rentschler, and G. A. Timco, *Chem.-Eur. J.* **8**, 277 (2002).
- <sup>16</sup>R. H. Laye, F. K. Larsen, J. Overgaard, C. A. Muryn, E. J. L. McInnes, E. Rentschler, V. Sanchez, S. J. Teat, H. U. Güdel, O. Waldmann, G. A. Timco, and R. E. P. Winpenny, *Chem. Commun. (Cambridge)* **2005**, 1125 (2005).
- <sup>17</sup>S. Carretta, P. Santini, G. Amoretti, M. Affronte, A. Ghirri, I. Sheikin, S. Piligkos, G. Timco, and R. E. P. Winpenny, *Phys. Rev. B* **72**, 060403(R) (2005).
- <sup>18</sup>S. Carretta, J. van Slageren, T. Guidi, E. Livioti, C. Mondelli, D. Rovai, A. Cornia, A. L. Dearden, F. Carsughi, M. Affronte, C. D. Frost, R. E. P. Winpenny, D. Gatteschi, G. Amoretti, and R. Caciuffo, *Phys. Rev. B* **67**, 094405 (2003).
- <sup>19</sup>T. Guidi, S. Carretta, P. Santini, E. Livioti, N. Magnani, C. Mondelli, O. Waldmann, L. K. Thompson, L. Zhao, C. D. Frost, G. Amoretti, and R. Caciuffo, *Phys. Rev. B* **69**, 104432 (2004).
- <sup>20</sup>B. Furniss, A. Hannaford, P. Smith, and A. Tatchell, *Vogel's Textbook of Practical Organic Chemistry*, 5th ed. (Longman Scientific & Technical, New York, 1989).
- <sup>21</sup>J. R. D. Copley and J. C. Cook, *Chem. Phys.* **292**, 477 (2003).
- <sup>22</sup>Go to <http://www.ncnr.nist.gov/dave>.
- <sup>23</sup>J. Schnack and M. Luban, *Phys. Rev. B* **63**, 014418 (2000).
- <sup>24</sup>O. Waldmann, T. Guidi, S. Carretta, C. Mondelli, and A. L. Dearden, *Phys. Rev. Lett.* **91**, 237202 (2003).
- <sup>25</sup>O. Waldmann, *Phys. Rev. B* **68**, 174406 (2003).
- <sup>26</sup>O. Waldmann, *Phys. Rev. B* **65**, 024424 (2001).
- <sup>27</sup>A. Chiolero and D. Loss, *Phys. Rev. Lett.* **80**, 169 (1998).
- <sup>28</sup>P. Santini, S. Carretta, G. Amoretti, T. Guidi, R. Caciuffo, A. Caneschi, D. Rovai, Y. Qiu, and J. R. D. Copley, *Phys. Rev. B* **71**, 184405 (2005).
- <sup>29</sup>A. Honecker, F. Meier, D. Loss, and B. Normand, *Eur. Phys. J. B* **27**, 487 (2002).